mathematics

Article

Associated Fault Diagnosis of Power Supply Systems Based on Graph Matching: A Knowledge and Data Fusion Approach

Laifa Tao [1,2,3], Haifei Liu [1,2,3], Jiqing Zhang [4], Xuanyuan Su [1,2,3], Shangyu Li [1,2,3], Jie Hao [5], Chen Lu [1,2,3], Mingliang Suo [1,2,3] and Chao Wang [1,2,3,*]

1 Institute of Reliability Engineering, Beihang University, Beijing 100191, China
2 Science & Technology on Reliability & Environmental Engineering Laboratory, Beijing 100191, China
3 School of Reliability and Systems Engineering, Beihang University, Beijing 100191, China
4 China International Engineering Consulting Corporation, Beijing 100048, China
5 AVIC Xi'an Flight Automatic Control Research Institute, Xi'an 710076, China
* Correspondence: wangchaowork@buaa.edu.cn

Abstract: With the rapid development of more-electric and all-electric aircraft, the role of power supply systems in aircraft is becoming increasingly prominent. However, due to the complex coupling within the power supply system, a fault in one component often leads to parameter abnormalities in multiple components within the system, which are termed associated faults. Compared with conventional faults, the diagnosis of associated faults is difficult because the fault source is hard to trace and the fault mode is difficult to identify accurately. To this end, this paper proposes a graph-matching approach for the associated fault diagnosis of power supply systems based on a deep residual shrinkage network. The core of the proposed approach involves supplementing the incomplete prior fault knowledge with monitoring data to obtain a complete cluster of associated fault graphs. The association graph model of the power supply system is first constructed based on a topology with characteristic signal propagation and the associated measurements of typical components. Furthermore, fault propagation paths are backtracked based on the Warshall algorithm, and abnormal components are set to update and enhance the association relationship, establishing a complete cluster of typical associated fault mode graphs and realizing the organic combination and structured storage of knowledge and data. Finally, a deep residual shrinkage network is used to diagnose the associated faults via graph matching between the current state graph and the historical graph cluster. The comparative experiments conducted on the simulation model of an aircraft power supply system demonstrate that the proposed method can achieve high-precision associated fault diagnosis, even under circumstances where there are an insufficient number of samples and missing parameters.

Keywords: deep residual shrinkage network; association graph model; knowledge and data fusion; Warshall algorithm; power supply system

MSC: 94C12

check for updates

Citation: Tao, L.; Liu, H.; Zhang, J.; Su, X.; Li, S.; Hao, J.; Lu, C.; Suo, M.; Wang, C. Associated Fault Diagnosis of Power Supply Systems Based on Graph Matching: A Knowledge and Data Fusion Approach. *Mathematics* **2022**, *10*, 4306. https://doi.org/10.3390/math10224306

Academic Editor: Yolanda Vidal

Received: 2 October 2022
Accepted: 14 November 2022
Published: 17 November 2022

1. Introduction

Decades ago, the ideas of more-electric aircraft (MEA) and all-electric aircraft (AEA) came into being [1]. In AEA, not only would all replaceable systems be replaced by electrical systems, but the propulsion power would also use electrochemical energy (e.g., batteries and fuel cells). At the same time, electrification has increased the supply of electric energy. With the continuous development of aircraft electrification, the requirements for the quality of aircraft power supply are increasing. Meanwhile, the complexity of aircraft power systems is also gradually increasing, which leads to higher requirements for the safety, maintainability, reliability, and testability of aircraft power supply systems [2,3].

Fault diagnosis is one of the important links in fault prediction and health management technologies [4,5]. Its purpose is to identify whether the system's working state is normal and whether it has deteriorated using intelligent algorithms in a certain working environment by combining the system's historical status information, fault information, working condition information, and other multi-source information, as well as historical parameter data. Then, fault isolation and location according to data characteristics can be realized [6,7]. Due to the complexity of the technical conditions of modern industrial processes, the influence of internal interaction loops is becoming increasingly prominent. When one monitoring variable is abnormal, it can easily cause changes in other monitoring variables through the relationships between faults, thus leading to related faults [8]. As a result, it is important to be able to analyze the fault source and locate the fault based on the numerous alarm data and their relationships. Power supply systems have such characteristics in real life. Therefore, the problem we aim to solve in this paper is how to correlate fault diagnosis and fault location through the node characteristics of the power supply system and their correlations.

There are mainly four kinds of fault diagnosis methods for power supply systems: knowledge-based [9,10], model-based [11,12], data-driven, and fault detection and diagnosis methods based on external equipment [13–15]. The model-based fault diagnosis method can mathematically express the research object and reveal the fault generation mechanism through the mathematical model. However, it is difficult to account for the coupling between components and their interactions with the environment during the modeling process. This results in models with limited ability to represent real faults and a high level of model complexity [16–18].

The data-driven fault diagnosis algorithm needs many historical data samples to support the model construction and training process. However, power supply systems have problems, such as difficulty obtaining fault samples, sample imbalance, etc. In addition, many data-driven algorithms lack certain physical meaning and interpretability, which makes it difficult to further apply and popularize the algorithm model. Data driven models, such as deep learning models, involve a large amount of computation and complex super parameters. How to further deploy them is also a problem to be considered [19–23]. The fault diagnosis of power supply systems based on external equipment is mainly carried out by actively applying different signals, via the system performance under different states, or through fault diagnosis rules. The authors of [24] proposed a development and implementation method for a permanent magnet synchronous motor controller for safety-critical applications. The authors of [25] proposed a method of fault diagnosis for aircraft secondary power distribution systems based on multi-valued logic and added cable fault detection and location functions to a traditional solid-state power controller.

The knowledge-based fault diagnosis method mainly uses knowledge to establish a diagnosis model. It performs fault inference analysis using object mechanisms, structure–function relationships, qualitative parameter analyses, and historical fault diagnosis experiences. Fault diagnosis expert systems and qualitative model-based methods are widely used [26–28]. However, in recent years, knowledge is used to remedy the problem of insufficient fault information in the data-driven model, to improve the adaptability and diagnostic ability of the model, and to make the model more targeted. The knowledge is supplemented in a data-driven way to improve the efficiency of model construction. At present, knowledge and data fusion is still in the exploration stage, and there are few related research achievements. Its main methods can be roughly divided into two categories: knowledge and data fusion model based on graph theory and knowledge and data fusion method based on the evidential reasoning model.

In association fault diagnosis, existing methods tend to focus on the correlation between parameters, the temporal relationship of fault propagation, and the probabilistic correlation of fault occurrence [29–34]. For special objects such as power supply systems, the parameter forms are often voltage, current, impedance, etc. The signal characteristics are relatively simple. It is difficult to analyze the association relationship only through parameters, and the propagation speed of current signals is fast. It is difficult to directly analyze the association between faults through time series, and the confidence of the probability association between faults is low when the data are incomplete. Therefore, we can summarize the urgent problem in the field of fault diagnosis as how to combine the advantages of data-driven and knowledge-driven models to quickly diagnose and locate faults through the correlations of components in different fault modes and their association patterns [35].

To solve the above problem, this paper proposes a high-level construction method of typical associated fault patterns of power supply systems based on a graph model. Based on anomaly monitoring and fault path tracking, the proposed method supplements the incomplete prior fault knowledge with monitoring data to obtain a complete cluster of associated fault graphs and realizes the fusion of knowledge and data. The main innovation points and contributions of this study can be summarized as follows:

(1) A knowledge and data fusion approach is proposed to diagnose the associated faults of power supply systems. The anomaly monitoring and fault path tracking based on the Warshall algorithm utilize historical data to supplement the incomplete prior fault knowledge, which establishes the complete cluster of typical associated fault mode graphs and realizes the organic combination and structured storage of knowledge and data.
(2) The proposed graph-matching strategy based on a deep residual contraction network achieves high precision with regard to fault diagnosis, even under the circumstances of an insufficient number of samples and missing parameters. The comparative experiments verify the depth feature extraction ability of the proposed method, as well as its high accuracy, noise resistance, and robust diagnostic capability.
(3) The proposed method preliminarily realizes deep association diagnosis and path backtracking under the condition of insufficient traditional FMEA knowledge and incomplete association information and provides an effective technical approach to solve accurate online fault diagnosis under strong coupling in the power supply system.

The remainder of this paper starts with a preliminary overview in Section 2. Then, Section 3 describes the two main methods of this study, including the association graph model based on knowledge and data fusion and the enhancement of component-associated knowledge based on the Warshall algorithm. The case studies in Section 4 show the process of the diagnosis of associated faults in power supply systems. The results indicate the priority of the methods in terms of accuracy under normal and missing-parameter situations. The paper closes with the main conclusions in Section 5.

2. Preliminary Overview

2.1. Warshall Algorithm

Definition 1. *Set digraph $G = \langle V, E\rangle$, set vertex $V = \{v_1, v_2, \ldots, v_n\}$, set edge $E = \{e_1, e_2, \ldots, e_n\}$, and define the adjacency matrix of digraph G as:*

$$A = (a_{ij})_{n\times n}, \tag{1}$$

where, a_{ij} is the number of edges adjacent v_i to the vertex v_j, $i = 1, 2, \ldots, n$, $j = 1, 2, \ldots, n$.

The Warshall algorithm is an algorithm for finding the transitive closure of adjacency [36]. In order to solve the problem of the large computation of the reachable matrix, the algorithm starts from the adjacency matrix A to obtain the matrix sequence $A, A_1, A_2, \ldots, A_n$. In order to judge the reachable path of each node in the matrix, the intermediate elements are fixed. Through the traversal of the intermediate elements, the path between two points is found to meet the requirement that only the nodes in the middle pass through $\{v_1, v_2, \ldots, v_k\}$ so that the algorithm only needs to perform sub addition n^3

times and sub multiplication n^3 times without matrix iteration. As a result, the number of calculations is reduced effectively. The algorithm steps are as follows [37]:

Step 1: Set matrix $F = A$, where A represents the adjacency matrix, 1 represents that there are edges between nodes, and 0 represents that there are no edges between nodes;

Step 2: Set $i = 1$;

Step 3: For any j, if $F[j,i] = 1$, then $F[j,k] = F[j,k] + F[j,i]$, where $k = 1,2,\ldots,n$;

Step 4: i plus 1;

Step 5: If $i < n$, go to Step 2;

Step 6: The algorithm ends.

The final matrix F is the reachable matrix, which can determine whether there is a path in the two nodes. If there is a path, it is represented by 1, and if not, it is represented by 0.

The Warshall algorithm will be used in Section 3.2 to achieve associated knowledge enhancement and updates on component associations based on abnormality monitoring and fault path retrieval so that the organic integration and structured storage of knowledge and data are realized.

2.2. Frechet Distance

The Frechet distance is a curve similarity measure algorithm. It considers not only the similarity of curves but also the distance between the data points of curves. It can evaluate the correlation between curves comprehensively, with the advantages of high diagnostic accuracy, speed, and adaptability [38,39]. Its calculation is described below.

The Frechet distance starts by calculating the values of the metric functions of different data points of a curve to the points on another curve. Then, the maximum values of the different metric functions are used as the set of Frechet distances to be determined. The final Frechet distance is the value of the lower bound of the Frechet distance to be determined. To calculate the Frechet distance, first set the binary group (S,d) as a metric space, where d is a metric function of S. Thus, the strict mathematical definition of the Frechet distance is as follows [40]:

Definition 2. *Set the binary group (S,d) as a metric space, where d is a metric function of S. To define the Frechet distance, the following conditions must be met:*

(1) The mapping γ of F on the unit interval $[0,1]$ is continuous.

(2) The vector ξ is mapped from the unit interval to itself, i.e., $\xi : [0,1] \to [0,1]$, and the mapping relation has the following conditions: the mapping function is continuous non-degenerate and ξ is full projective, at which point the function ξ is said to be a reparametrized function of the unit curve $[0,1]$.

(3) Let A and B be two continuous curves on S; that is, $A : [0,1] \to S$, $B : [0,1] \to S$. $d(x)$ is the metric function of S. Then, let α and β be two reparametrized functions of the unit interval. Then, the Frechet distance $F(A,B)$ of the curves A and B is defined as:

$$F(A,B) = \inf_{\alpha,\beta,t\in[0,1]} \max\{d(A(\alpha(t)), B(\beta(t))\}, \tag{2}$$

The Frechet distance is sometimes referred to as "leash distance". As is shown in Figure 1, the dog walks along its own set trajectory between the owner and the dog, the owner's trajectory is A, the dog's trajectory is B. There is a rope between the owner and the dog to constrain the longest distance between them. During the travel, the Frechet distance is the minimum value of the rope that can ensure both can move along the trajectory.

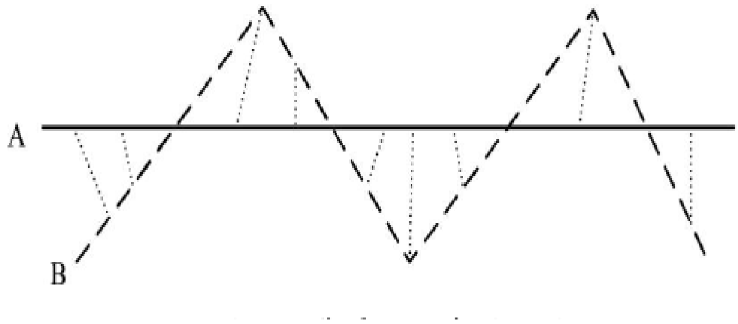

Figure 1. Typical structure diagram of convolutional neural network.

In this study, the optimal correlation analysis method needs to be selected to have the best correlation fuzzy metric effect, which can differentiate different modes. In a normal state, the correlation between the input signal and output signal of a component should be kept within a certain range, and when a fault occurs, the distance will change. Thus, the identification of different fault modes can be achieved based on the change in correlation.

The Frechet distance is used in the following correlation metric-based component fault diagnosis method. Typically, a distance metric is applied to the range of values and curve similarity between the operating parameters and the normal parameters. Then, we determine the extent to which the parameter deviates from the normal operating conditions combined with a distance threshold. When the distance value deviates from the threshold value, the component can be identified as abnormal.

2.3. Deep Residual Shrinkage Network

2.3.1. Convolutional Neural Networks (CNN)

Convolutional neural network is a classical deep learning model, which adds convolution to the traditional network to extract features. With development, it is now utilized in not only image processing but natural language and time series handling. Some widely used CNN models are LeNet-5, AlexNet, VGGNet, ResNet and so on [41,42].

A typical CNN contains three major layers, namely, a convolutional layer, pooling layer and fully connected layer. The network uses gradient descent to minimize the loss function for the purpose of adjusting the weight parameters in the network layer by layer, and the accuracy of the network is improved through iterative back-propagation training. LeNet-5 does not have an input layer. There are 7 layers in total, including 5 hidden layers (excluding pooling layers), that is, the number of layers that can train parameters is 5. VGGNet is mainly proposed to solve the problem that Lenet's recognition of large size pictures is not satisfactory. Compared with LeNet, AlexNet has a deeper network structure, with a total of eight hidden layers, including five convolutional layers and three full connection layers. However, although AlexNet has a good effect, it does not give the design direction of deep neural network, that is, how to make the network deeper. VGGNet strictly uses 3×3 small-scale convolution and pooling layer to construct depth of CNN, achieving good results. Small convolution can reduce parameters and facilitate stacking convolution layers to increase depth, that is, deepen the network and reduce convolution. At the same time, there is another network, ResNet, which uses the residual connection structure to make the network deeper from the perspective of avoiding gradient disappearance or explosion. There are five versions in total, of which ResNet-18 is the 18-layer version.

2.3.2. Deep Residual Network

In traditional CNNs, due to the complexity of the input parameters, it is often necessary to increase the depth of the model in order to improve the feature extraction capability and classification ability of the model. When too many hidden layer structures are added to the network structure, it may lead to a problem of gradient disappearance and step explosion. During the construction of the model, the parameters of each iteration of the model need to be back-propagated. The important operation during back propagation is the derivation of the gradient from the model error. The gradients will be accumulated and piled up in the network. As the number of hidden layers increases, the gradient will grow or decay exponentially with the number of layers, which is the phenomenon of gradient explosion and gradient disappearance. This will affect the running speed of the model and the classification effect.

As a new deep learning method, the core contribution of a deep residual network (ResNet) is to introduce the idea of identity mapping to the traditional network structure [43]. The core idea is to transfer the features of shallow data to the deep network through identity mapping so that the deep network contains the feature information of the shallow mesh structure, which greatly reduces the probability of gradient disappearance and gradient explosion, thus enhancing the feature extraction ability of the network model [44]. The specific structure is shown in Figure 2. When data are input, on the one hand, the data will pass through the residual path and a residual network is built on the residual path. After the input data pass through the path, a residual item $F(x)$ will be obtained, and the data x will also be output through the identity mapping model. Currently, the learned feature is $x + F(x)$. The goal of the residual network is to fit the residual term $F(x)$.

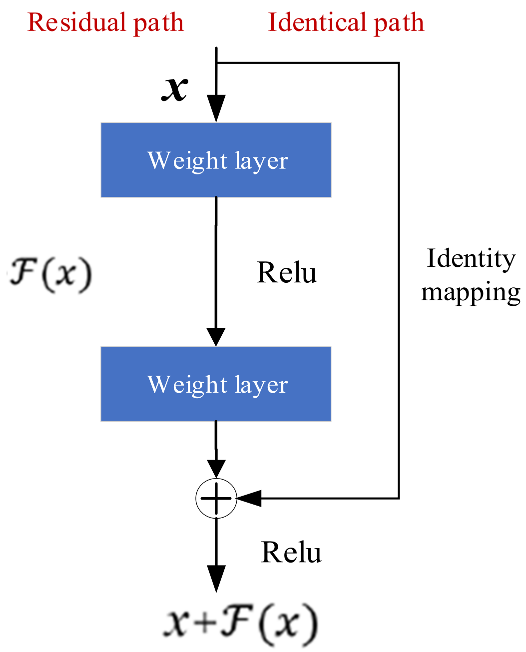

Figure 2. Schematic graph of residual unit.

By increasing the residual units, the training difficulty of the network parameters in the model is greatly reduced through the same path, the feature extraction ability of the original CNN is enhanced, the gradient disappearance and gradient explosion problems in the model are greatly reduced, and a model with stronger classification ability is trained to better adapt to complex data conditions.

2.3.3. Deep Residual Shrinkage Network

In general, the collected data often contain noisy information and redundant parameters unrelated to the target problem due to the limitations of the data collection methods or the influence of the working environment. It will affect the output accuracy of the model on the one hand and the operation efficiency of the model on the other. To solve this problem, the deep residual reduction network improves the original residual module based on the above-mentioned deep residual network. Additionally, the influence of target-independent features on the results is minimized by adding a soft thresholding operation. That is, features with absolute values less than the threshold are assigned to 0 by a nonlinear transformation in the soft thresholding operation, which "shrinks" the redundant features in the direction of 0, thus enabling feature selection [45]. Referring to the related article [46,47], the basic structure of the deep residual reduction network is as follows (Figure 3):

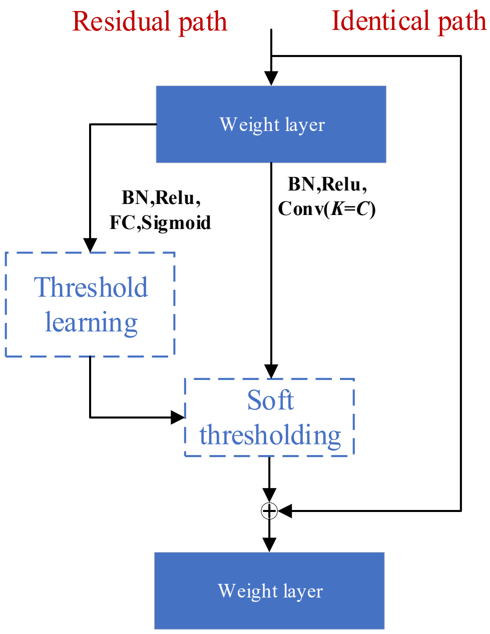

Figure 3. Basic structure of deep residual shrinkage network.

The principle of the soft threshold function is as follows:

$$y = \begin{cases} x - thr & x > thr \\ 0 & -thr \le x \le thr \\ x + thr & x < -thr \end{cases}, \tag{3}$$

where x represents the input feature, y represents the output feature, and thr represents the threshold value.

In the neural network model, a gradient operation is required for the features of each layer; that is, the derivation of the above formula. The results are as follows:

$$\frac{\partial y}{\partial x} = \begin{cases} 1 & x > thr \\ 0 & -thr \le x \le thr \\ 1 & x < -thr \end{cases}, \tag{4}$$

It can be seen that soft thresholding can limit the gradient to 0 and 1, thus preventing the problem of gradient disappearance and gradient explosion. Additionally, it can be seen that the key problem of soft thresholding is the acquisition of a threshold, and the self-learning of a threshold for different features can reduce sample noise and redundant feature interference, which is an advantage of deep residual shrinkage networks.

The threshold value in the residual shrinkage network is obtained by using the absolute operation and the GAP layer (global average pooling layer) to simplify the feature and convert it into a one-dimensional vector. The feature is marked as $A = \{a_{jic}\}$, where i, j, c represent the length, width, and number of channels of the input feature map, respectively. On the other hand, features are propagated to the two-layer full connection layer network (FC layer). Finally, the output of the FC network is scaled to the range of (0,1) via the following formula:

$$\alpha = \frac{1}{1 + e^{-z}}, \tag{5}$$

where α represents the scaling coefficient and z represents the characteristics of neurons. Thus, the expression of the threshold value can be obtained as follows:

$$\tau = \alpha \cdot \text{average}|a_{i,j,c}|, \tag{6}$$

where τ represents the calculated threshold value. In the deep residual shrinkage network, the threshold value τ must be positive and cannot be greater than the maximum absolute value of the feature map. Otherwise, according to the formula, the final output will be 0. Through this soft thresholding method, the threshold value can be kept within a small positive range. Due to the special structure of the depth residual shrinkage network, each sample can form a set of thresholds according to its own characteristic graph so that noise and redundant features can be reduced for specific samples.

The deep residual shrinkage network and the other neural networks mentioned are used in this work to conduct the mining and classification of features for the cluster of associated fault modes and to diagnose the current operating conditions in the power supply system. The comparison of different networks is shown by case studies in Section 4.

3. Proposed Method

There are two core steps of the proposed method. First, the initial graph models for different fault modes are established by extracting features sensitive to fault information and combining them with a priori knowledge of the power supply systems. Secondly, through data-driven correlation metrics and path tracking, model enhancement for correlated faults is achieved, which complements the absence of priori knowledge about associated faults and provides the main innovation of the proposed method.

3.1. Association Graph Model Based on Knowledge and Data Fusion

Since most of the currents generated in the power supply system are AC signals with high frequency and high fluctuation characteristics, the processing methods using time domain signals are often prone to loss of information. Thus, the pre-processing of the signal is required to extract the required fault state characteristic information from the complex signal. Commonly used signal analysis methods include time domain analysis, frequency domain analysis, and time-frequency domain analysis. This paper utilizes the Hilbert–Huang (HHT) transform-based time-frequency domain signal feature extraction method to analyze the signals and extract the features more adequately. At the same time, this paper also performs signal feature extraction via RMS, which is an important parameter to characterize the energy and stability of AC signals in circuit analysis.

The HHT transform can decompose high-frequency signals and obtain the instantaneous frequency and instantaneous amplitude of the signals. The RMS feature, as a common parameter in circuit analysis, can reflect the trend of circuit energy changes over time. Therefore, the feature extraction method in this study can obtain the feature information of data from three aspects: frequency, amplitude, and trend, which can achieve the retention or even enhancement of the fault characteristics.

Next, we build the association graph model based on knowledge and data fusion. There is a wide range of associations between components in the power supply system, and the associations are often distinguished in different operating states. Therefore, graph models can be established to describe the component associations in different operating states. There are two objectives, which are to realize the backtracking of abnormal component propagation paths under different associated fault states and to realize fault diagnosis based on the associated characteristics of components under different fault states. Specifically, there are many components in the power supply system, and there are natural physical connections between the components. In order to describe the association relationships of components in the power supply system, the components in the power supply system are regarded as nodes, while the association metrics between components are regarded as edge weights in the graph model to ultimately obtain an undirected weighted graph (defined as follows).

Definition 3. *Undirected weighted graph means that the edges in the graph model are undirected and weighted. The so-called undirected refers to any point pair* (i, j) *and* (j, i)*corresponding to the same edge, and vertex i and vertex j are also called the two endpoints of the undirected edge. The adjacency matrix of the undirected weighted graph G is:*

$$A = (a_{ij})_{n \times n}, \tag{7}$$

where a_{ij} *is the weight of the edge* v_j *adjacent to the vertex* v_i, $i = 1, 2, \ldots, n, j = 1, 2, \ldots, n$.

By analyzing the association between components in different fault modes, we obtain the association diagram model of the power supply system in different states. Meanwhile, the actions of various power controllers inside the power supply system can affect or block the propagation of fault signals, so the association of components in fault states may occur outside the physical structure. Therefore, it is necessary to combine the associated fault states together.

Since the electrical energy of the power supply system is generated by the primary power supply and then transmitted to the supply load through the secondary power supply, it can be assumed that the fault signal of the component is also propagated along the direction of electrical energy transmission. Therefore, the propagation direction of the electrical signal can be added to the original undirected weighted graph to create a directed weighted graph. The directed weighted graph gives directions to the edges based on the undirected weighted graph, which can further characterize the bidirectional propagation relationship between nodes. Therefore, the association graph model of the power supply system is constructed by combining the knowledge of the functional structure and the current transmission direction, as is shown in Figure 4. In the constructed association graph model, the transmission direction of the electrical signal is specified by the direction of the arrow and represented by the association degree results of the components. The system topology is simplified by the physical connection associations of the components. In the figure below, the yellow part indicates the components of the main power supply equipment of each channel, including the auxiliary exciter, rectifier bridge, main exciter, rotary rectifier, and main motor; light green indicates the next layer of signal transmission, including the AC load and each transformer rectifier; brown indicates the rectification part of each transformer rectifier; dark green indicates each transformer rectifier; red indicates each bus; and blue indicates each DC load. The hierarchical representation of the association graph allows the transmission level and direction to be clearly seen, providing support for further analysis.

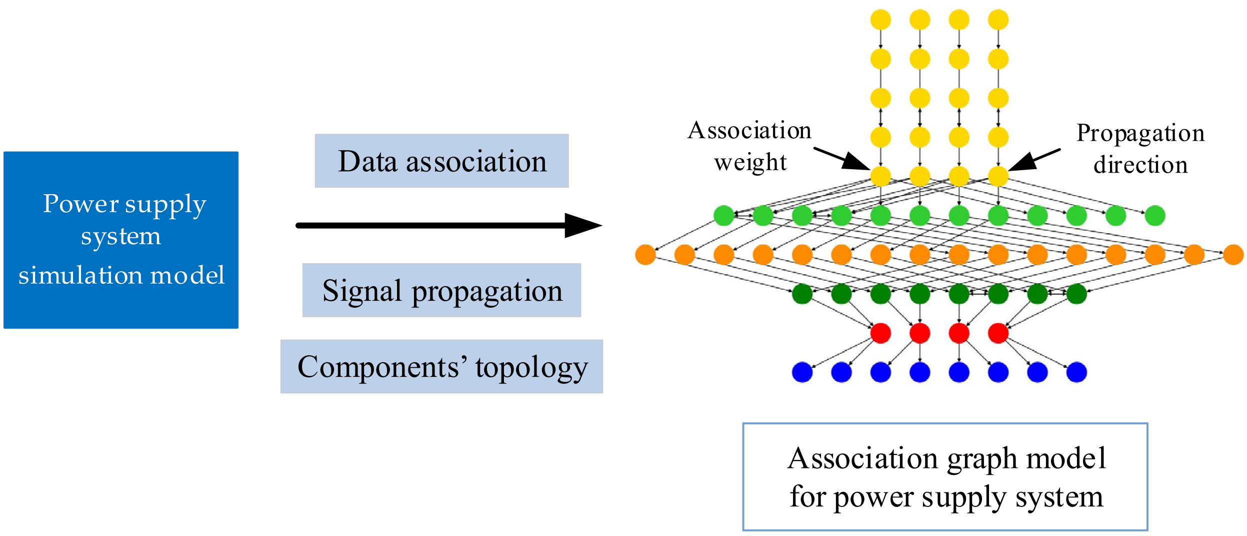

Figure 4. Reconstruction and reduction of the power supply system association graph model.

The graph model visually represents and structures the associations between components through nodes and edges so that the graph model can be used as an identification criterion for different fault modes. Thus, the identification of associated fault modes can be realized in Section 4.

3.2. Enhancement of Component Associated Knowledge Based on the Warshall Algorithm

The associated faults in the power supply system are often caused by the transmission of fault signals from the fault source to the associated components, resulting in a drift in the monitoring signals of the components. Additionally, this causes association alarms, making it difficult to identify the fault source and diagnose the fault mode. However, the topology of the power supply system is already determined. When the data are incomplete, it is difficult to fully explore the associations between the components due to the influence of monitoring noise and the uncertainty of the operating mode present in the data. The situation gets worse when the knowledge is incomplete as well. Although the association graph model of the power supply system developed in 3.1 can locate the fault source to a certain extent, the presence of the power controller still often affects or hinders the propagation of the fault signals due to the complexity of the associated faults. In the association fault model, there will always be components associated with the power supply system outside of its physical structure. Therefore, it is necessary to enhance the association knowledge based on component anomaly detection.

Definition 4. *Set digraph $G = \langle V, E \rangle$, set vertext $V = \{v_1, v_2, \ldots, v_n\}$, set edge $E = \{e_1, e_2, \ldots, e_n\}$, and define the adjacency matrix of digraph G as:*

$$A = (a_{ij})_{n \times n}, \tag{8}$$

where a_{ij} is the number of edges adjacent v_i to the vertex v_j, $i = 1, 2, \ldots, n, j = 1, 2, \ldots, n$.

In the directed graph, if a node can reach the target node through other nodes in the graph, it is considered that there is a reachable path between the node and the target node. Then, the existing alarm component set can be analyzed through the directed graph, the fault propagation path can be inferred with, and the fault source can be found. In this paper, the accessibility matrix is used to trace the source of typical associated fault modes, and thus the knowledge of the association graph model can be enhanced.

The accessibility matrix of digraph G is:

$$P = (P_{ij})_{n \times n}, \tag{9}$$

where $p_{ij} = 1$ if and only if the vertex v_i can reach the vertex v_j, otherwise $p_{ij} = 0$, $i = 1, 2, \ldots, n$, $j = 1, 2, \ldots, n$.

In this paper, Warshall's method is used to calculate the accessibility matrix and to further enhance the knowledge of the association graph model. The algorithm flow is as follows (Figure 5):

Firstly, the graph model is structured and stored according to the power supply system association graph model through the adjacency matrix. Secondly, the accessibility matrix is calculated through the Warshall algorithm to analyze the accessibility path of the association graph model. Then, according to the actual detection parameters of the power supply system, component fault detection based on association measurement is carried out, and a set of associated fault alarm components is obtained. According to the hierarchical structure of the association graph model, the accessibility path traversal of the alarm component set is performed in reverse (i.e., from the load level to the main power level). When the path cannot be traced forward, the last backtracking point is considered as the fault source under a certain path.

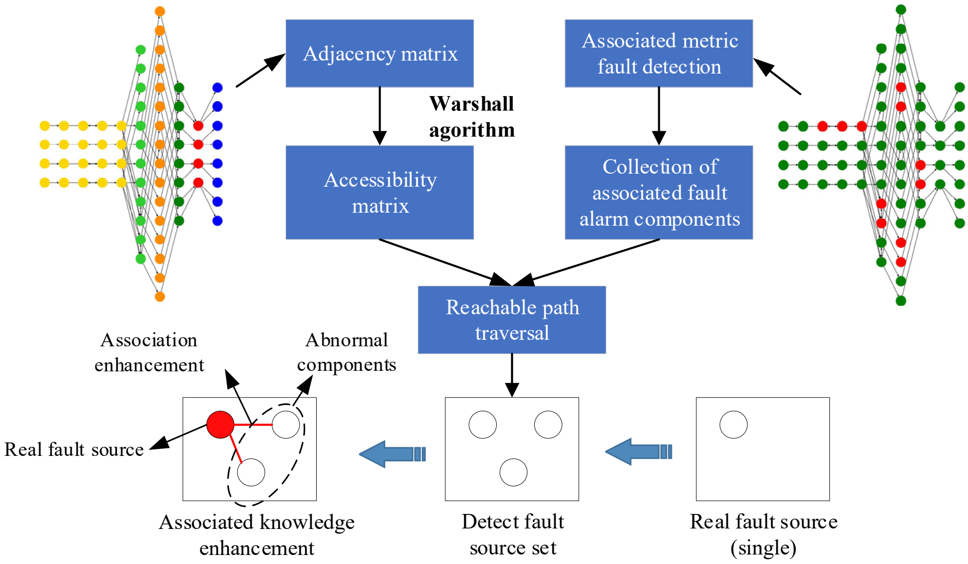

Figure 5. Knowledge enhancement process of power supply system association graph model.

In addition, with the association measurement algorithm based on Frechet distance proposed in this paper, the associations between different components can be obtained and applied to fault feature classification and fault diagnosis. Therefore, in the association graph model of the power supply system, the associations between components, i.e., weights, can be replaced by the association measurement results, thus organically combining data and knowledge. In addition, the graph structure can be stored in matrix form via adjacency matrices. Each adjacency matrix can be considered a graph. Multiple data under each associated fault mode can be considered a cluster of graphs. Multiple data under multiple associated fault modes can form a typical cluster of associated fault mode graphs. Component associations and signaling under different associated fault modes are stored to form a knowledge base to provide a basis for fault diagnosis. The associated fault mode clusters are defined as follows:

$$Graph = [g_{ij}]_{f \times n}, \tag{10}$$

$$g = [Frechet(a,b)]_{m \times m}, \tag{11}$$

where g_{ij} represents the j-th graph under the mode of the i-th associated fault mode; $Frechet(a,b)$ represents the Frechet-associated metric between component a and component b, f represents the number of fault modes in the clusters, n represents the number of fault samples, and m represents the number of power supply system components included in the clusters.

4. Case Studies

4.1. Construction of the Simulation Model

The data in this paper come from an aviation AC main power supply simulation model. This paper combines research data and experimental verification to construct a simulation model of a typical aircraft four-channel power supply system based on the Simulink tool in MATLAB. Moreover, this paper also combines the real parameter data of the power supply system provided for model modification and improvement. In this model, four three-phase alternators are used to supply power, which constitute a constant-speed and constant-frequency AC power supply system, and its four AC channels are not connected in parallel. The secondary power supply uses variable voltage rectifiers for a 270 V variable voltage rectifier and a 28 V variable voltage rectifier, and each is connected to one 270 V variable voltage rectifier and one 28 V variable voltage rectifier (high voltage and low voltage), respectively. At the same time, the first and second channels' DC power supply comes through the convergence bar for power integration, and the third and fourth channels' DC power supply comes through the convergence bar for power integration. The DC power supplies are connected to two hydraulic pump loads (high voltage loads, working in parallel) and two resistors (low voltage loads, working in parallel). There are also four AC loads in the system, represented by two three-phase resistors, which are connected to four generators. The simulation model graph of the power supply system is as follows (Figure 6):

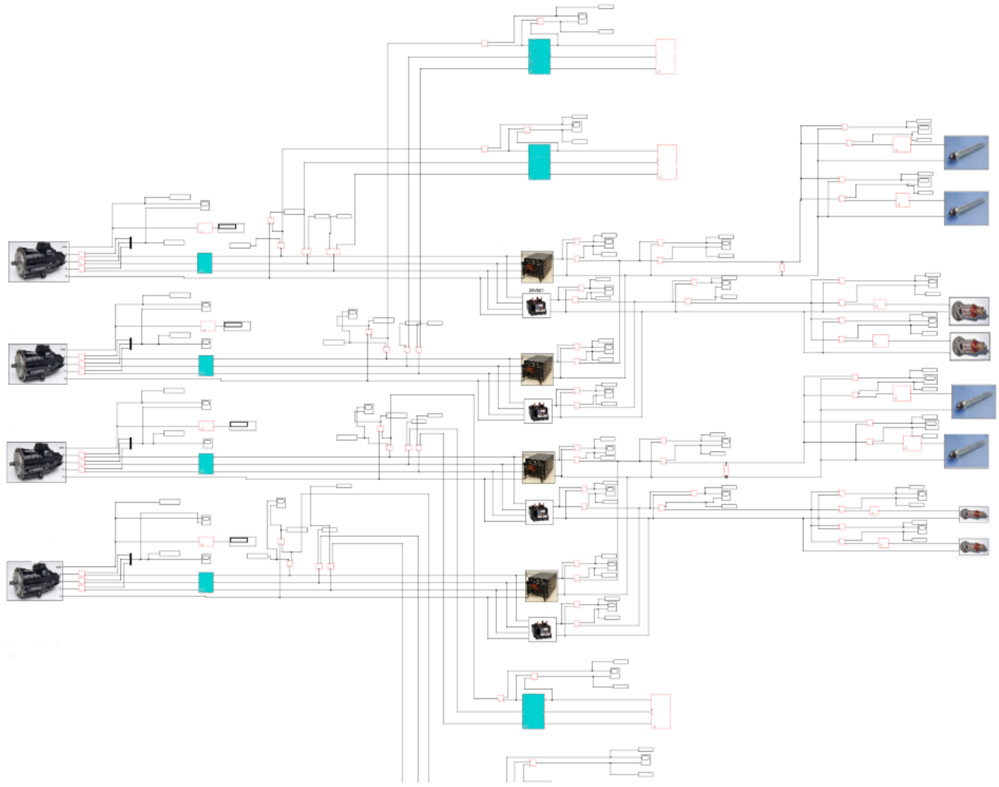

Figure 6. Power supply system simulation model.

In the power supply system structure used in this paper, the four channels of AC power are independently powered and connected to the AC load, while the DC power is sinked and distributed through the DC sink bar. In order to analyze the power supply modes in different channels and to obtain the complete data characteristics, the circuit switching logic in the fault state is not considered in this study.

In order to realize the fault characterization and parameter change analysis of the power supply system under different fault modes, it is necessary to collect and analyze the parameters of each component at each level. Therefore, a total of 218 measurement points including the power supply system level, equipment level, and component level are added to this model in order to monitor the status of 4 levels, 12 pieces of equipment, and 60 components in the power supply system.

4.2. Establishment of the Associated Fault Diagnosis Model

This paper uses the deep residual contraction network model to carry out fault diagnosis based on the power supply system's associated fault mode graph. The model construction process is shown in Figure 7.

First, construct a cluster of associated fault modes based on the topological knowledge and historical parameter information. Second, construct a deep residual shrinkage network model based on the residual shrinkage network units. Third, complete the training of the fault diagnosis model library based on the cluster of associated fault modes. Then, generate an association graph based on the actual measured parameters. The process uses the association metric analysis technique of actual monitoring parameters and the association graph model. Finally, input the association graph into the trained deep residual shrinkage network model for diagnosis and obtain the diagnosis results.

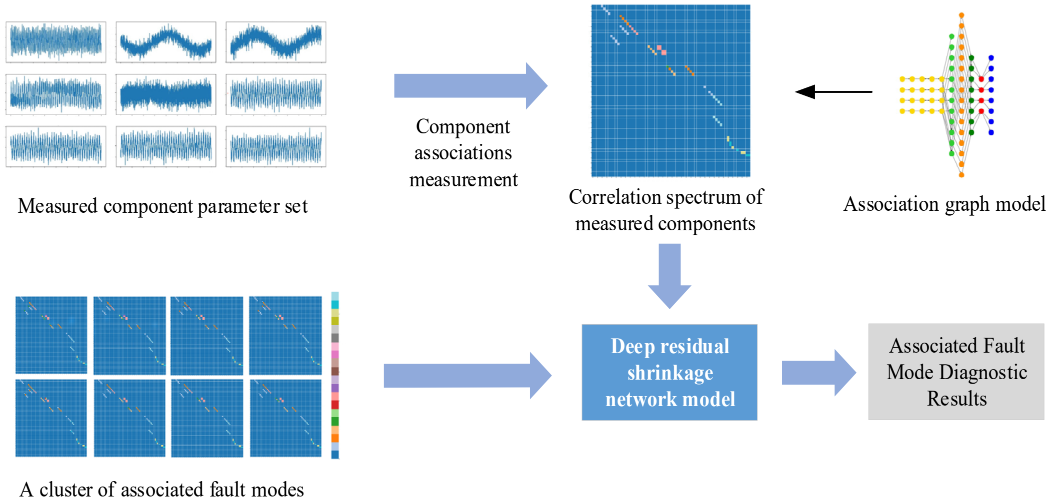

Figure 7. Schematic graph of power supply system associated fault diagnosis model.

To start with, we proceed with the associated fault detection based on the Frechet distance metric. The purpose is to obtain the set of abnormalities in each fault mode and to visually display the associated graph model. The associated fault detection results of a typical power supply system under the first channel are shown in Figure 8. The green nodes in the figure represent components with normal parameters and the red nodes represent components with abnormal parameters. From the results, it can be seen that when the associated faults occur, the fault source and the associated components will have abnormal parameters to some extent.

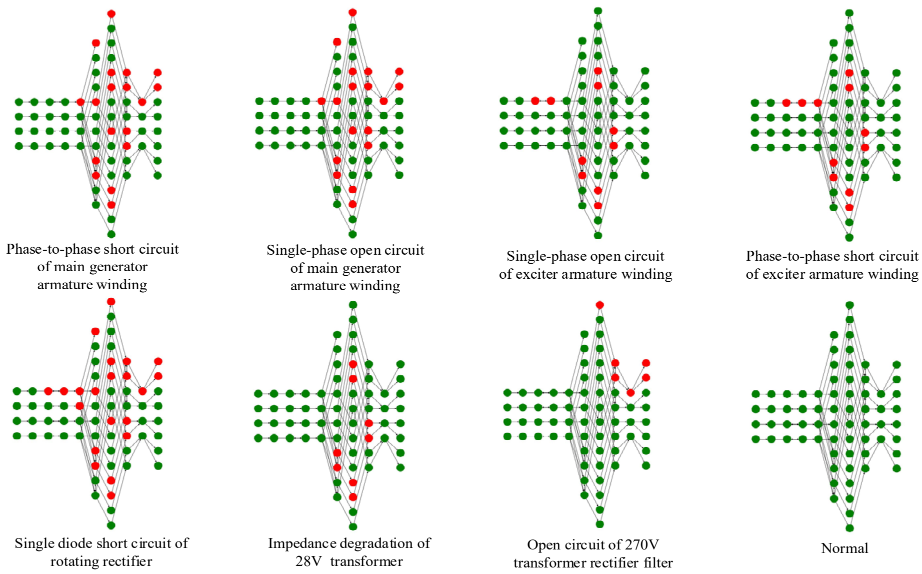

Figure 8. Detection results of associated faults of typical power supply systems.

The following conclusions can be drawn from the analysis of the associated fault detection results:

(1) Under different associated fault modes, the sets of abnormal components caused by different associations are different due to the complexity of the power supply system connection structure, functional composition, and transmission mode. It is difficult to comprehensively analyze the component associations under different associated faults using only a simple power supply system structure.

(2) In the power supply system, the association direction of the fault-related components caused by the fault source is not only related to the power supply system structure. Due to the incomplete selection of the electrical energy control and component acquisition parameters of the generator controller in the power supply system, associations outside the power supply system structure often occur. For example, a phase-to-phase short-circuit fault in the armature winding of the main generator, No. 1, causes a fault not only in low-voltage transformer No. 1 but also in low-voltage transformer No. 2. This is because the low-voltage DC bus of the power supply system is converged by transformers No. 1 and No. 2. Therefore, it is necessary to strengthen the associations of the association graph model of the power supply system according to the fault detection results in different fault modes.

(3) In typical associated faults of the power supply system, the propagation direction of the fault signal is not necessarily unidirectional. For example, the open-circuit fault of a single diode of the rotating rectifier can also cause a parameter shift for the exciter. Therefore, when constructing the association graph model, it is also necessary to consider the associations of the bi-directional connected components.

(4) The associations of each component of the power supply system need to further rely on component anomaly detection analysis and fault path back analysis. This is to analyze and strengthen the association features such as transmission direction of fault signals and component association outside the physical structure in the power supply system so as to improve the feature extraction capability and fault diagnosis capability of the model.

Further, the enhancement of component-associated knowledge is performed based on knowledge and data fusion. Take the phase-to-phase short-circuit fault in the armature winding of the exciter of the power supply system as an example. Figure 9 shows the backtracking path and fault source detection after the accessible path traversal of the fault alarm set. As can be seen from the fault alarm component set, the fault in the exciter armature winding is transmitted to the 28 V transformer rectifier through the rotating rectifier and the main motor, causing a series of associated fault representations. The red path is the fault tracing path consistent with the true fault source, while the yellow path can only be traced back to LV transformer #2. In fact, there are two sources of faults, the main exciter #1 and the LV transformer #2. This indicates that, due to the generator controller, the fault signal from the rectification of transformer #1 28 V may affect the rectification of transformer #2 28 V in order to ensure that the current and voltage of the circuit meet the target requirements, thus causing a deviation in the parameters of transformer #2 LV. Therefore, the associations under the fault path should be considered in the association graph model. The research content of this paper assumes that the fault source of the associated fault mode in the power supply system is a single fault source or a double fault source of the same component. Therefore, the associations of the original association graph model are enhanced by the blue path, thus further improving the ability of the model to represent the overall state of the power supply system.

The association graph model of the power supply system constructed in this paper is further updated with knowledge through the fault path retrieval and association enhancement under each typical associated fault mode. Further, the model is more capable of representing the associations of components under different fault states, thus further enhancing the fault diagnosis capability. The improved association graph model of the power supply system is shown in Figure 10. In the updated association model, the clusters of the components are not changed. However, the fault path retrieval based on the Warshall algorithm enhances the association knowledge of the components. On the one hand, the association direction of the components is supplemented with the original edges; on the other hand, the association outside the physical structure shown by the components, i.e., the edges in the graph, is enhanced in the associated fault mode.

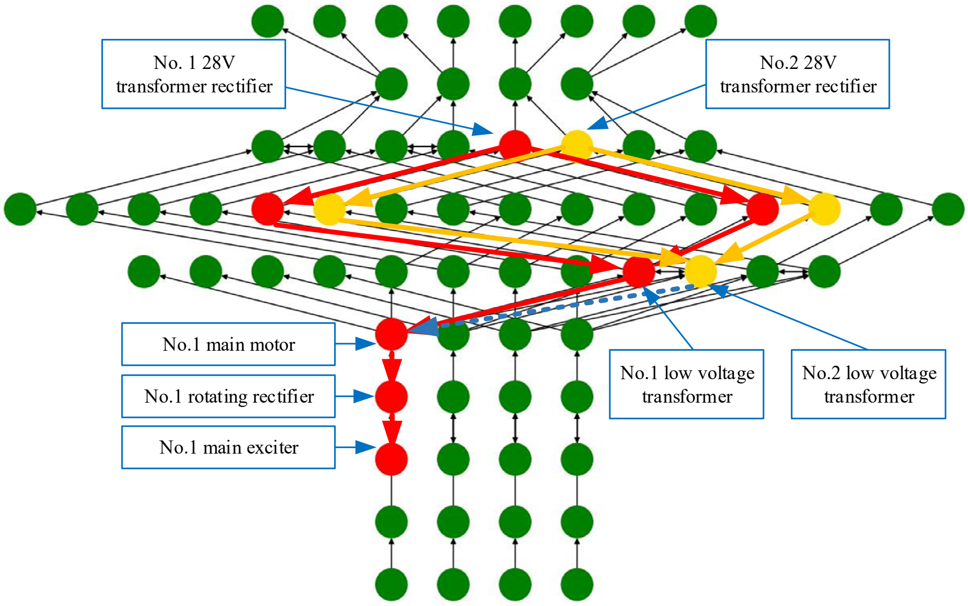

Figure 9. Example graph of phase-to-phase short-circuit fault backtracking of exciter armature winding.

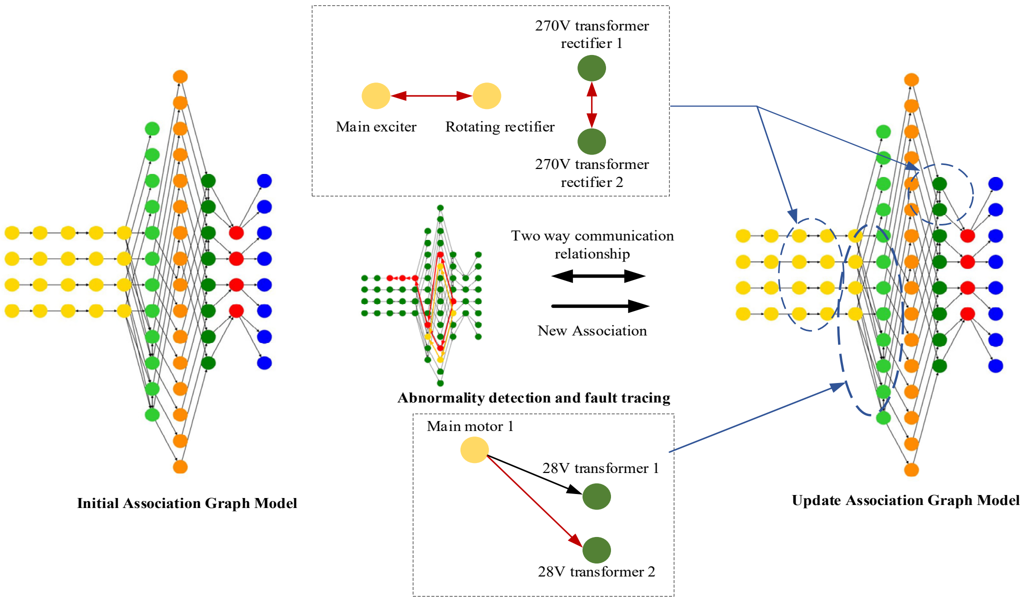

Figure 10. The power supply system's association graph model.

Then, we obtain the results of a cluster of associated fault modes based on the Frechet distance and the Warshall algorithm.

In the graphs, the horizontal and vertical coordinates represent the serial numbers of the components, respectively, and the weight corresponding to the coordinates (a, b) is the weight of the associated measurement between component a and component b, as shown in Table 1.

In Figure 11, different colors represent the weights of each aspect, which means that the differences in association measurements between components can be shown. As can be seen from the figure, both the basic structure of the cluster of association modes and the connection topology between components remain unchanged, which is mainly because the structure of the association graph model does not change. Nevertheless, the associations between components change under different fault modes, and the weights of the edges change accordingly. Figure 12 shows a comparison of the associated fault graphs under normal conditions and under the phase-to-phase short-circuit of the excitation armature winding.

Table 1. Associated mode cluster component serial number name comparison table.

No.	Components	No.	Components	No.	Components	No.	Components
0	Pilot exciter 1	17	Main motor 2	34	High variable filter 13	51	270 V regulating 4
1	Pilot exciter 2	18	Main motor 3	35	High variable filter 14	52	28 V regulating 1
2	Pilot exciter 3	19	Main motor 4	36	Low variation filter 11	53	28 V regulating 2
3	Pilot exciter 4	20	AC load 1	37	Low variation filter 12	54	28 V regulating 3
4	Rectifier bridge 1	21	AC load 2	38	Low variation filter 13	55	28 V regulating 4
5	Rectifier bridge 2	22	AC load 3	39	Low variation filter 14	56	High voltage busbar 1
6	Rectifier bridge 3	23	AC load 4	40	High variable filter 21	57	High voltage busbar 2
7	Rectifier bridge 4	24	High voltage transformer 1	41	High variable filter 22	58	Low voltage busbar 1
8	Main exciter 1	25	High voltage transformer 2	42	High variable filter 23	59	Low voltage busbar 2
9	Main exciter 2	26	High voltage transformer 3	43	High variable filter 24	60	Fuel pump 1
10	Main exciter 3	27	High voltage transformer 4	44	Low variation filter 21	61	Fuel pump 2
11	Main exciter 4	28	Low voltage transformer 1	45	Low variation filter 22	62	Fuel pump 3
12	Rotating rectifier 1	29	Low voltage transformer 2	46	Low variation filter 23	63	Fuel pump 4
13	Rotating rectifier 2	30	Low voltage transformer 3	47	Low variation filter 24	64	Heater 1
14	Rotating rectifier 3	31	Low voltage transformer 4	48	270 V regulating 1	65	Heater 2
15	Rotating rectifier 4	32	High variable filter 11	49	270 V regulating 2	66	Heater 3
16	Main motor 1	33	High variable filter 12	50	270 V regulating 3	67	Heater 4

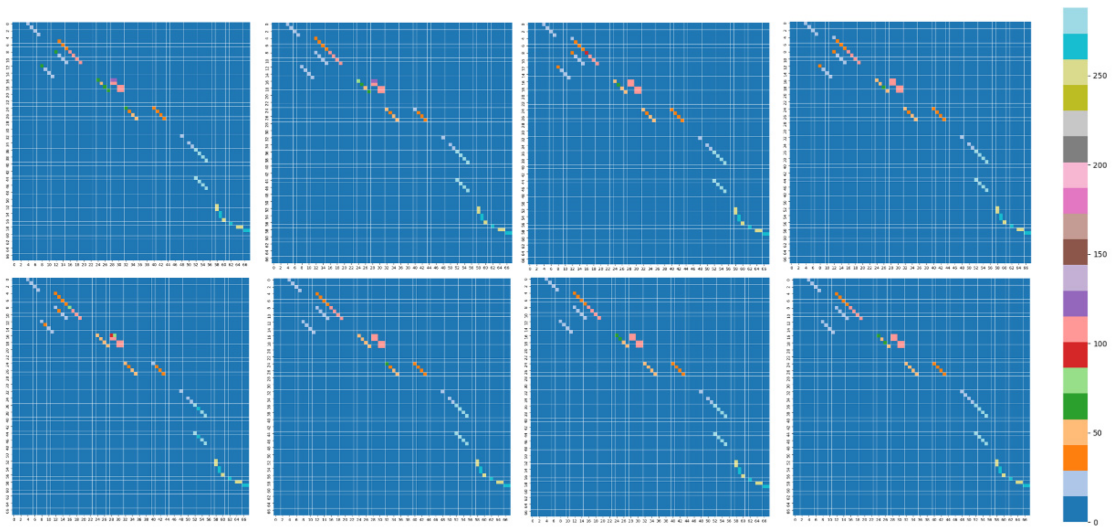

Figure 11. Schematic graph of a cluster of associated fault mode results.

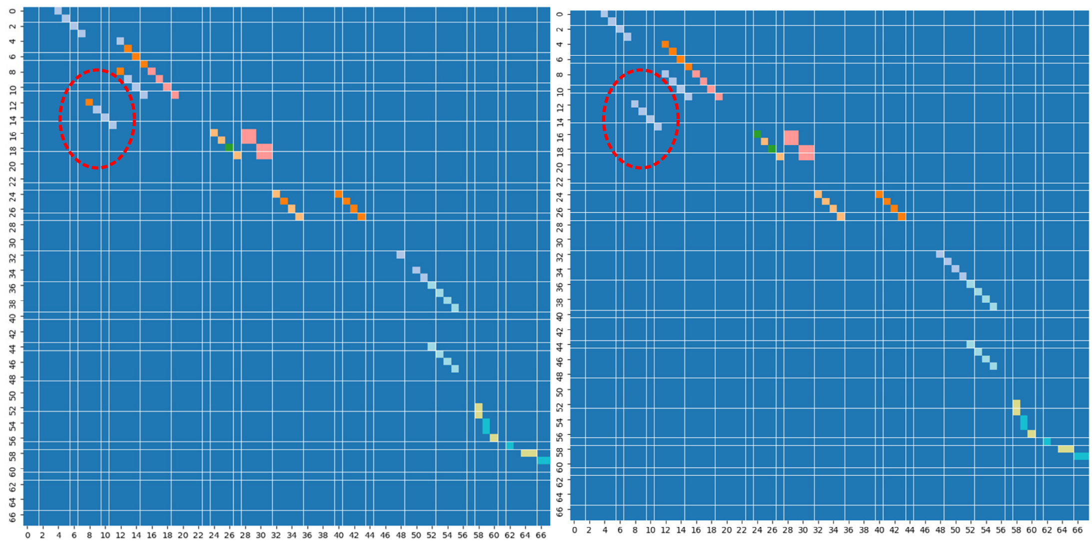

Figure 12. Comparison of associated fault graph.

As is shown in Figure 12, the associations of the components highlighted in the two graphs have changed, and the coordinates are (8, 12) and (12, 8), respectively. In the graphs, 4 represents No. 1 main exciter and 12 represents No. 1 rotating rectifier. The change also verified that the armature winding of the exciter has a phase-to-phase short-circuit fault and further verified the rationality and interpretability of the construction of the graphs.

Based on this, this study constructs a cluster of typical associated fault modes of the power supply system, organically integrates the structural knowledge of the power supply system, signal propagation direction, and parameter characteristics, and realizes the enhancement of data-based associations. Finally, structured storage is carried out. On the one hand, the associations and signal propagation relationship of each component of the power supply system can be obtained through the graphs, and on the other hand, the characteristics of the components are deeply extracted. The graphs can directly reflect the changes in component associations caused by the change of parameter characteristics under different fault conditions, thus saving storage space and providing a basis for improving the efficiency of the diagnosis model.

4.3. Diagnosis Results and Analysis

4.3.1. Data Introduction

In this part, the relevant fault diagnosis models of the power supply system are validated using simulation modeling of a typical aircraft power supply system and data sets created in fault injections. The data set includes seven typical fault injections: phase-to-phase short-circuit in the main generator armature winding, single phase open-circuit in the main generator armature winding, single phase open-circuit in the exciter armature winding, phase-to-phase short-circuit in the exciter armature winding, single diode short-circuit in the rotary rectifier, impedance attenuation in the 28 V transformer rectifier, and open-circuit and normal in the 270 V transformer rectifier filter inductor. Together with the fault data of single-fault point injections and double-fault point injections, there are 42 fault modes. By adding Gaussian noise with a signal-to-noise ratio of 5, 50 sets of samples are generated for each fault mode, and 43 sets of associated fault mode hierarchies for different fault types are generated by the above method of constructing the associated mode hierarchies for power supply systems. Each group has 50 graphs as training and testing data for the deep residual shrinkage network.

4.3.2. Operating Environment

In this section, the deep residual systolic network model is built by PyTorch, and the model is trained and validated. Compared with other deep learning frameworks, the PyTorch framework has the advantages of simple design and high operational efficiency. The fault diagnosis model related to power supply systems based on a deep residual systolic network proposed in this study is built with PyTorch 1.9.0.

4.3.3. Diagnosis Results

In this section, a network model based on deep residual shrinkage is constructed for a power supply system-associated fault diagnosis. Forty sets of samples are used as the training and validation sets, and the last 10 sets of samples are used as the test set for model testing and validation. The model is trained for 300 iterations, and the convolution kernel parameter is set to 3. The training loss and final confusion matrix during model training are shown in Figures 13 and 14.

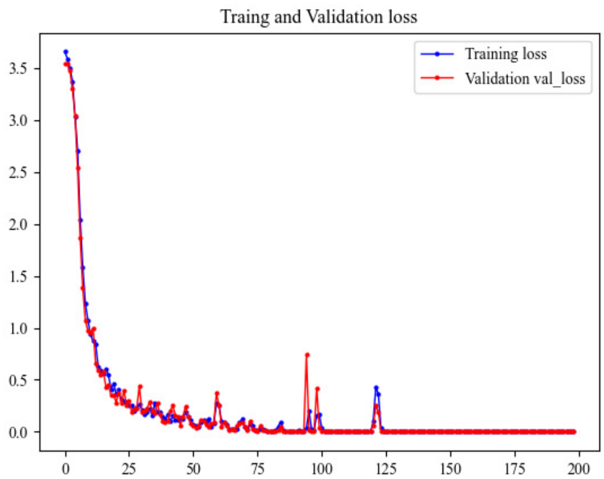

Figure 13. Training loss in the process of associated fault diagnosis.

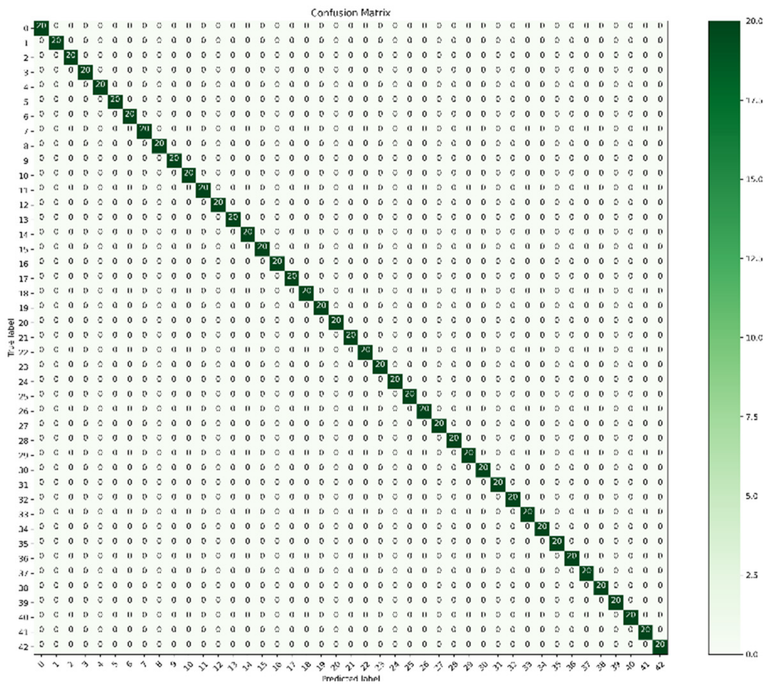

Figure 14. Confusion matrix in the process of associated fault diagnosis.

From the above fault diagnosis results, it is apparent that, on the one hand, the deep residual shrinkage network model constructed in this paper can realize the feature mining and classification of the association fault pattern graphs. Moreover, due to the soft threshold and identity mapping in the deep residual unit, the model converges faster and can effectively reduce the redundant information and noise interference in the graph model, and the accuracy rate of association fault diagnosis reaches 100%. On the other hand, it can be seen from the loss function that the trend of the loss function of the training set is basically consistent with that of the validation set. This indicates that the associated fault mode mapping of the power supply system in this paper can still construct data features with strong consistency under the condition of noise, which means it can be used for fault diagnosis.

4.3.4. Validation and Comparison

To further verify that the correlation metric based on the Frechet distance in this paper is optimal, the effects of several common correlation metrics are compared. Here, the correlation metric is calculated and the results are analyzed using the parameters under different fault modes, such as exciter output voltage and rotating rectifier input voltage, selected from normal conditions, exciter armature winding phase short circuit, exciter armature winding open circuit, main generator armature winding single phase open circuit, rotating rectifier single diode open circuit, and 28 V varactor impedance degradation. The different algorithms are evaluated using three parameters: intra-cluster sum of squares, contour coefficients, and CH metrics. The mathematical definitions of the several methods are as follows:

(1) Cluster sum of square

$$CSS = \sum_{j=0}^{m}\sum_{i=1}^{n}(x_i - \mu_i)^2, \tag{12}$$

n represents the number of data points in each class, m represents the number of clusters, x_i represents the data points, and μ_i represents the mean value of each class.

(2) Contour coefficient

$$S(i) = \frac{b(i) - a(i)}{\max(a(i), b(i))}, \tag{13}$$

where $a(i)$ denotes the average distance from each point i to other points in the cluster and $b(i)$ denotes the average distance from each point to all other points in the cluster.

(3) Calinski–Harabaz index (CH)

$$\mathrm{CH}(k) = \frac{\mathrm{BGSS}}{K-1} / \frac{\mathrm{WGSS}}{n-K} \tag{14}$$

$$\mathrm{WGSS} = \frac{1}{2}\left[(n_1 - 1)\overline{d}_1^2 + \cdots + (n_\kappa - 1)\overline{d}_K^2\right] \tag{15}$$

$$\mathrm{BGSS} = \frac{1}{2}\left[(K-1)\overline{d}^2 + (n-K)A_K\right] \tag{16}$$

$$A_K = \frac{1}{n-K}\sum_{i=1}^{n}(n_i - 1)\left(\overline{d}^2 - \overline{d}_i^2\right) \tag{17}$$

where n is the number of samples in the data set, K is the number of categories, $\overline{d}_j^2$ is the average distance between samples in the j-th category, $j = 1, 2, \cdots, k$, and $\overline{d}^2$ is the average distance between all samples. A larger CH indicator indicates that the clustering result is more concentrated within clusters and more dispersed between clusters, i.e., there is a better clustering effect.

In this paper, the correlation analysis method is used to achieve the correlation measure of components in different states from the parameter level. Common correlation analysis methods are as follows:

(1) Pearson's correlation coefficient

Pearson correlation coefficient is a common analysis index in vector similarity analysis [48–51] that is mainly used to portray the linear correlation between two vectors. A coefficient output result of 0 means that there is no correlation between two vectors, a positive result means a positive correlation, and a negative result means a negative correlation. Its calculation formula is as follows:

$$\begin{aligned} \rho_{X,Y} &= \frac{\operatorname{cov}(X,Y)}{\sigma_X \sigma_Y} = \frac{E((X-\mu_X)(Y-\mu_Y))}{\sigma_X \sigma_Y} \\ &= \frac{E(XY)-E(X)E(Y)}{\sqrt{E(X^2)-E^2(X)}\sqrt{E(Y^2)-E^2(Y)}} \end{aligned}, \tag{18}$$

(2) Parametric analysis based on the gray correlation analysis model

The basic idea of gray correlation analysis is to reflect the correlation between parameters through the degree of similarity of the curve geometry between the data of each parameter [52–55]. It is mainly applied to the description and analysis of the developmental changes between parameters within the system [56]. Let the reference series be $X_o(t)$ and the comparison series be $X_i(t)$, then the gray correlation degree is calculated as.

$$\eta_i(t) = \frac{m + \rho M}{\Delta_i(t) + M}, \ \rho \in [0,1], \tag{19}$$

where $\Delta_i(t) = |x_0(t) - x_i(t)|$, $i = 1,2,\cdots m$, $t = 1,2,\cdots,n$, $M = \max(\Delta_i(t))$, $m = \min(\Delta_i(t))$.

(3) Mahalanobis distance

The Mahalanobis distance is a method of measuring the similarity between two sample sets starting from the perspective of the distribution characteristics of the sample set [57–60], and its main feature involves considering the connection between different features to be able to be independent of the measurement scale. It is often used to measure the distance between multidimensional time series parameters, and the Mahalanobis distance between the data vectors x and y is:

$$D_{\mathrm{M}}(x,y) = \sqrt{(x-y)^{\mathrm{T}} \sum\nolimits^{-1} (x-y)}, \tag{20}$$

where $\sum^{-1}$ is the covariance matrix of the multidimensional random variables.

(4) Cosine similarity

The cosine similarity measures the cosine of the angle between the vectors by converting the parameters into vectors to determine the consistency of the direction between the two vectors, which further determines the correlation of the parameters [61–64]. Therefore, this method is commonly used to determine the consistency of the variation between two parameters. The range of values is between -1 and 1, with -1 indicating that the two vectors are the exact opposite and 1 indicating that they are exactly the same. The cosine similarity between sequence X and sequence Y is:

$$\operatorname{sim}(X,Y) = \cos\theta = \frac{\sum\limits_{i=1}^{n} (X_i \times Y_i)}{\sqrt{\sum\limits_{i=1}^{n} X_i^2 \times \sqrt{\sum\limits_{i=1}^{n} Y_i^2}}}, \tag{21}$$

(5) DTW (dynamic time warping algorithm)

The DTW (dynamic time warping) algorithm, commonly used for speech similarity recognition, has the main advantage of being able to measure the similarity of two time series data, especially two data of different lengths, through a dynamic planning algorithm [65–68]. The basic algorithm of dynamic time regularization is as follows. Assuming that two time series are X and Y, set their lengths as n and m, respectively, where:

$$\begin{aligned} X &= x_1, x_2, \ldots, x_i, \ldots, x_n \\ Y &= y_1, y_2, \ldots, y_j, \ldots, y_m \end{aligned} \tag{22}$$

To calculate the shortest path between the two, first construct a $n \times m$ path matrix W where each element in the matrix corresponds to the Euclidean distance between the two points, i.e.,:

$$w = d\left(x^{th}, y^{th}\right), \tag{23}$$

$$d\left(x_i, y_j\right) = \sqrt{\left(x_i - y_j\right)^2}, \tag{24}$$

When the path matrix is constructed, the minimum cumulative distance between the two sequences, i.e., the DTW distance, is calculated as follows:

$$DTW(X, Y) = \min\left\{\sqrt{\sum_{K=1}^{K} w_k / K},\right. \tag{25}$$

where K is the number of alignment points and w_k is an element of the path matrix representing the distance between x and y in the k-th group of points.

A comparative situation analysis for each distance metric algorithm with different metric parameters is shown in Table 2:

Table 2. Associated mode clusters' component serial number name comparison table.

Metric Algorithm	CSS	Contour Factor	CH
Pearson correlation coefficient	3.4692	0.0536	199.5176
Grey correlation analysis	11.6526	−0.1574	21.9299
Mahalanobis distance	5.0645	0.6025	116.6640
Cosine similarity	0.5429	0.1715	2694.7450
Dynamic Time Warping	0.0080	0.7599	343,059.7323
Frechet distance	0.0001	0.9425	15,413,927.6165

From the comparison of the indicators, it can be seen that the clustering concentration of the Frechet distance is much higher than that of other algorithms, which proves that for the characteristic parameters of the power supply system in this paper, the Frechet distance can sharply identify the changes to the data in terms of curve trends and numerical distances so as to achieve more accurate fault diagnosis.

In more detail, firstly, the Pearson correlation coefficient and gray correlation analysis methods are used to measure the correlation between the change trends of two series. In this study, however, the data are characterized as stable variation data that maintain certain fluctuation characteristics, and it is difficult to analyze their correlation by variation trends, so it is difficult to distinguish different failure modes. Secondly, the Marxian distance and cosine distance can measure the similarity between two stable sample data; however, both have the disadvantage of not being sensitive to the absolute value of the specific value of the sample, i.e., the size of the data value has little effect on the results. However, through the aforementioned analysis, the current and voltage tend to change only numerically in certain fault modes and do not change in frequency, so it is difficult for both to achieve excellent results in certain fault modes. Both the dynamic time regularization algorithm and the Frechet distance analyze the correlation between parameters from the dimension of path similarity of time series, while it can be seen from the results that the Frechet distance has a better clustering effect.

To further verify the improvement in diagnostic capability brought by the deep residual shrinkage network proposed in this paper, two neural networks are tested additionally, including ResNet18 and basic CNN. These methods are commonly used after research [69–73]. The diagnostic accuracy and confusion matrix of each model is shown in Figures 15 and 16.

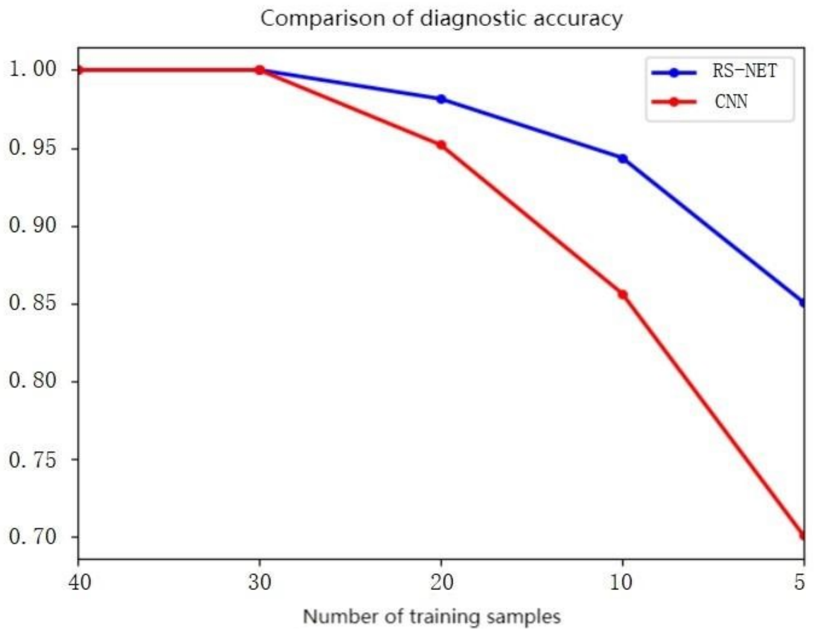

Figure 15. Comparison chart of fault diagnosis accuracy of two methods by number of samples.

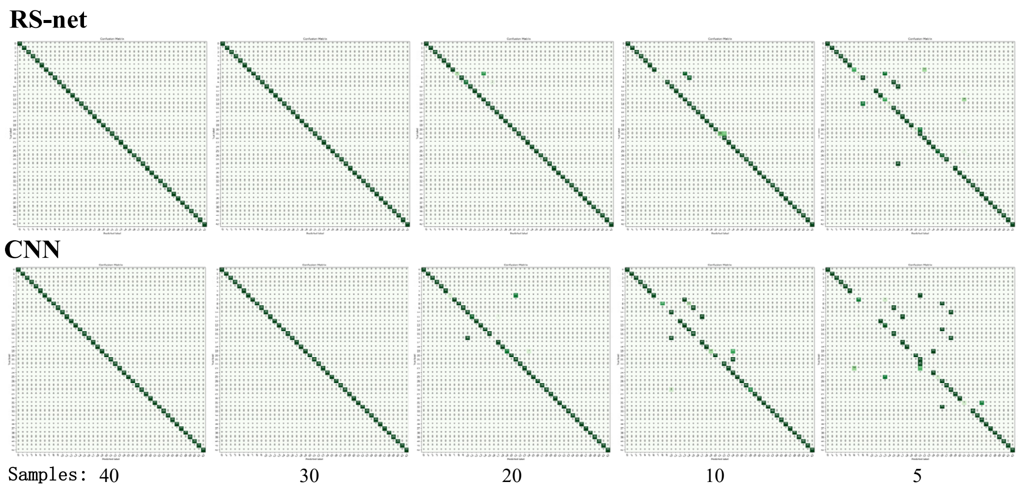

Figure 16. Comparison of confusion matrix of two methods with different numbers of training samples.

At the same time, we have adopted AutoGluon 0.5.2, which uses automatic super parameter adjustment, model selection or integration, architecture search and data processing to rapidly prototype the original data for deep learning and classical machine learning solutions. We applied some other nsetworks trained by AutoGluon, and obtained the accuracy results, whose values are all distributed between 0.7386 and 0.7727, far from 0.9907 of the deep neural shrinkage network proposed in this paper (Table 3).

Table 3. Accuracy results for several networks trained by AutoGluon.

No.	Model	Accuracy
1	WeightedEnsemble_L2	0.7727
2	RandomForestGini	0.7386
3	LightGBMXT	0.7636
4	CatBoost	0.7636
5	XGBoost	0.7705
6	LightGBMLarge	0.7568
7	NeuralNetTorch	0.7523
8	NeuralNetFastAI	0.7545
9	LightGBM	0.7409
10	KNeighborsUnif	0.7409
11	The proposed model	0.9907

The superiority of neural networks can be clearly seen from the results. From the comparison of the above diagnosis results, it can be seen that the associated fault diagnosis model based on the deep residual shrinkage network model proposed in this paper is significantly less affected by the size of the fault samples than the traditional CNN model. This is mainly because the residual shrinkage unit in the model reduces the interference of the model with redundant data and noise and can better achieve the feature extraction and classification of the associated fault mode graphs. Through the cross-sectional comparison of test results, the fault diagnosis accuracy of both can be maintained above 70% when the amount of data is only five groups. This can prove that the construction method of clusters of associated fault modes proposed in this paper can achieve robust fault feature extraction and structured storage of noisy parameter data and has excellent performance in terms of fault diagnosis. It can alleviate the problem of insufficient data samples under actual operating conditions.

To further verify the superiority of the association graph model, we apply the feature extraction results directly in three networks for training. Several classical machine learning models trained with AutoGluon including WeightedEnsemble_L2, RandomForestGini, KNeighborsUnif, SVM and XGBoost. The comparison of the diagnostic accuracy with and without the association graph model is shown below. We obtained the accuracy results of training samples of 5, 10, 20, 30 and 40, respectively, and averaged them (Table 4).

Table 4. Comparison of the diagnostic accuracy with and without the association graph model.

No.	Model	Accuracy with Graph Model	Accuracy without Graph Model
1	WeightedEnsemble_L2	0.7727	0.7341
2	RandomForestGini	0.7386	0.7341
3	KNeighborsUnif	0.7409	0.7386
4	SVM	0.7334	0.7080
5	XGBoost	0.7705	0.7293

It can be seen from the table that the association graph model has brought about improvement for all models, with 5.65% at most and 0.31% at least. This is because the association graph model integrates knowledge and data and has more information than the unstructured stored feature extraction results.

To further validate the feature extraction capability of the associated fault mode graphs of the power supply system proposed in this paper, specific fault points are removed in this paper. This is carried out to verify the robustness and accuracy of the feature extraction and fault diagnosis of the model in the absence of parameters. In the experiment, the data points of No. 1 main motor, No. 1 rectifier, No. 1 auxiliary exciter, No. 1 main exciter, and No. 1 rotary rectifier in the associated fault graph of the power supply system are set to zero to simulate the actual monitoring environment in which the monitoring parameters of No. 1 main power supply are missing in order to verify the fault diagnosis effect of the model under the condition of missing fault parameters. Figure 17 shows the graphs of the normal state before and after the missing parameters. From the figure, it can be seen that due to the missing parameters of the main power supply components, the points of the related fault mode graph are also missing.

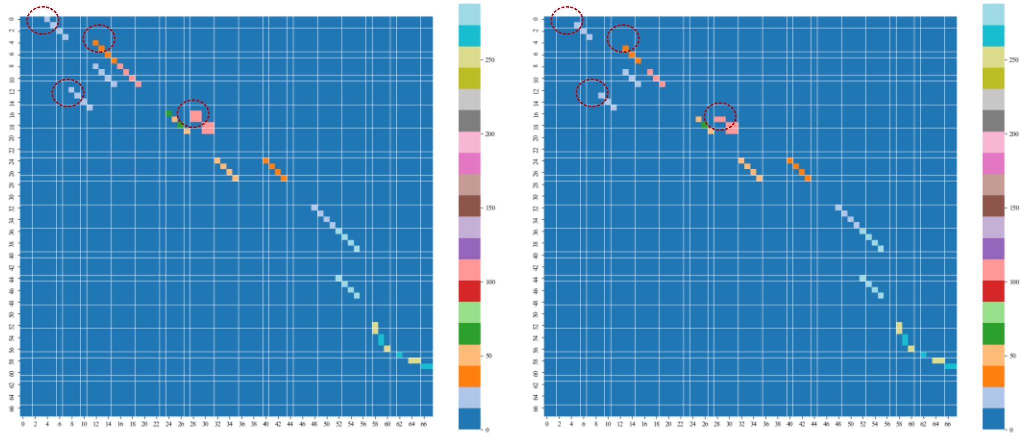

Figure 17. Comparison graph of normal state-associated fault mode graph before and after missing parameters.

In this paper, the training set and the test set are processed for parameter loss at the same time. With 40 groups of samples as the training set and 10 groups of samples as the test set, the deep residual shrinkage network model and CNN model are constructed and trained. The results of the confusion matrix are shown in Figure 18.

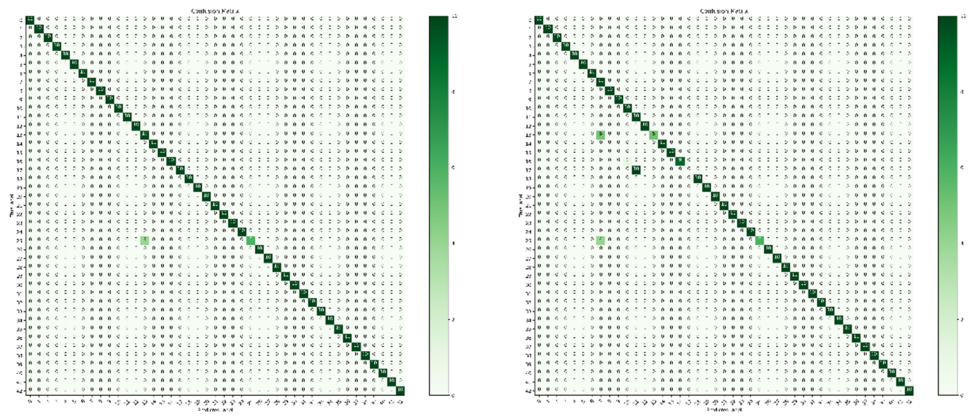

Figure 18. Comparison of the two confusion matrices in the case of missing parameters.

The test results show that the deep residual shrinkage network model constructed in this paper can achieve the diagnosis of typical associated fault modes with 99.07% accuracy, even when the main power parameters of the first channel are completely missing. In addition, the diagnosis accuracy by CNN reaches 95.35%, which reflects the robustness of the model for feature extraction in this paper. Due to the structural expression of component and parameter associations in the cluster, the graph model has the ability of feature extraction against parameter loss, thus adapting to the actual usage environment.

Further analysis reveals that in the confusion matrix of the deep residual shrinkage network, the misclassification of the model is mainly fault 13 and fault 25, which correspond to the phase-to-phase short-circuit in the first channel of the armature winding and the impedance drop fault in the first channel of the 28 V transformer rectifier, respectively. Since they are closely related to the main power supply parameters, some feature information is lost, leading to a decrease in the diagnostic accuracy of the model. The misclassification of the CNN is mainly for faults 7, 13, 11, 17, and 25, corresponding to the faults single-phase open-circuit of the excitation armature winding of the first channel, phase-to-phase short-circuit of the excitation armature winding of the first channel, impedance drop of the 28 V transformer rectifier of the first channel, phase-to-phase short-circuit of the excitation armature winding (first and second channels), and single-phase open-circuit of the excitation armature winding (first and second channels), respectively.

The experiment proves that the graph model-based component analysis and associated fault diagnosis model can solve the problems of information structured storage and complex feature extraction for power supply systems based on knowledge and data fusion. Additionally, it can realize accurate fault diagnosis of typical associated fault modes and achieve high accuracy diagnosis under the circumstances of insufficient samples and missing parameters. In short, the model has good robustness and adaptability.

5. Conclusions

This paper proposes a knowledge and data fusion approach for the associated fault diagnosis of power supply systems. Based on the graph model, the proposed approach organically combines the hierarchical structure, signal transmission direction, and data association relationship of the power supply system to construct the initial cluster of typical associated fault mode graphs, solving the problem of assigning data information to the power supply system structure and associating knowledge and parameters. Then, the accessibility matrix of the association graph model is calculated according to the Warshall algorithm, and the fault path set is obtained by backtracking the component fault detection results based on the association measurement. By comparison with the real fault source, the association relationship is updated and the incomplete prior fault knowledge is supplemented, establishing the final cluster of typical associated fault mode graphs. Finally, a deep residual reduction network model is constructed for graph matching, realizing the diagnosis of associated faults. Compared with other models, the proposed model can achieve more high-precision associated fault diagnosis, even under difficult situations such as insufficient sample size or missing parameters, demonstrating its robustness and adaptability.

Author Contributions: Data curation, J.Z.; Formal analysis, J.Z. and X.S.; Funding acquisition, C.L. and C.W.; Methodology, L.T. and H.L.; Writing—original draft, J.H. and C.W.; Validation, S.L. and M.S.; Investigation, X.S.; Supervision, C.W. All authors have read and agreed to the published version of the manuscript.

Funding: This study was supported by the National Natural Science Foundation of China (Grant Nos. 61973011 and 61903015), the Fundamental Research Funds for the Central Universities (Grant No. KG21003001), National key Laboratory of Science and Technology on Reliability and Environmental Engineering (Grant No. WDZC2019601A304), as well as the Capital Science & Technology Leading Talent Program (Grant No. Z191100006119029).

Conflicts of Interest: The authors declare no conflict of interest.

References

1. Weimer, J.A. Electrical power technology for the more electric aircraft. In Proceedings of the [1993 Proceedings] AIAA/IEEE Digital Avionics Systems Conference, Fort Worth, TX, USA, 25–28 October 1993.
2. Barzkar, A.; Ghassemi, M. Electric Power Systems in More and All Electric Aircraft: A Review. *IEEE Access* **2020**, *8*, 169314–169332. [CrossRef]
3. Thapa, N.; Ram, S.; Kumar, S.; Mehta, J. All electric aircraft: A reality on its way. *Mater. Today Proc.* **2021**, *43*, 175–182. [CrossRef]
4. Park, J.Y.; Lim, I.S.; Choi, E.J.; Kim, M.S. Fault diagnosis of thermal management system in a polymer electrolyte membrane fuel cell. *Energy* **2021**, *214*, 119062. [CrossRef]
5. Saeed, U.; Jan, S.U.; Lee, Y.D.; Koo, I. Fault diagnosis based on extremely randomized trees in wireless sensor networks. *Reliab. Eng. Syst. Saf.* **2020**, *205*, 107284. [CrossRef]
6. Wu, X.; Zhang, Y.; Cheng, C.; Peng, Z. A hybrid classification autoencoder for semi-supervised fault diagnosis in rotating machinery. *Mech. Syst. Signal Process.* **2021**, *149*, 107327. [CrossRef]

7. Vogl, G.W.; Weiss, B.A.; Helu, M. A review of diagnostic and prognostic capabilities and best practices for manu-facturing. *J. Intell. Manuf.* **2019**, *30*, 79–95. [CrossRef]
8. Jiang, Y.; Yin, S.; Kaynak, O. Optimized Design of Parity Relation Based Residual Generator for Fault Detection: Data-Driven Approaches. *IEEE Trans. Ind. Inform.* **2020**, *17*, 1449–1458. [CrossRef]
9. Lawhorn, D.; Rallabandi, V.; Dan, M.I. A Network Graph Technique for the Design of Electric Aircraft Power Systems. In Proceedings of the IEEE Transportation Electrification Conference and Expo, Chicago, IL, USA, 22–26 June 2020.
10. Meng, F.; Yang, S.; Wang, J.; Xia, L.; Liu, H. Creating Knowledge Graph of Electric Power Equipment Faults Based on BERT–BiLSTM–CRF Model. *J. Electr. Eng. Technol.* **2022**, *17*, 2507–2516. [CrossRef]
11. Ren, X.; Li, Y.; Wu, T.Y.; Qu, S.; Li, M. Fault Diagnosis of Complex Electric Power System Using the Improved Grey Incidence Degree Model. In Proceedings of the 2017 5th International Conference on Machinery, Materials and Computing Technology (ICMMCT 2017), Busan, Republic of Korea, 25–27 August 2017.
12. Zhang, Y.; Zhang, J.; Ma, J.; Wang, Z. Fault Diagnosis Based on BFS in Electric Power System. In Proceedings of the International Conference on Measuring Technology & Mechatronics Automation, Hunan, China, 11–12 April 2009.
13. Zhang, Z.; Jian, H.; Jiang, Y.; Geng, W.; Xu, Y. Overview and analysis of PM starter/generator for aircraft electrical power systems. *CES Trans. Electr. Mach. Syst.* **2017**, *1*, 117–131. [CrossRef]
14. Wang, B.; Vakil, G.; Liu, Y.; Yang, T.; Zhang, Z.; Gerada, C. Optimization and Analysis of a High Power Density and Fault Tolerant Starter-Generator for Aircraft Application. *Energies* **2020**, *14*, 113. [CrossRef]
15. Arumugam, P.; Dusek, J.; Aigbomian, A.; Vakil, G.; Bozhko, S.; Hamiti, T.; Gerada, C.; Fernando, W. Comparative design analysis of Permanent Magnet rotor topologies for an aircraft starter-generator. In Proceedings of the 2014 IEEE International Conference on Intelligent Energy and Power Systems, Kyiv, Ukraine, 2–6 June 2014.
16. Setlak, L.; Kowalik, R. Mathematical Modeling and Simulation Studies of Selected Components of the Electricity Generation, Processing and Distribution System of Aircrafts According to the Concept of More Electric Aircraft. In Proceedings of the 2018 International Symposium on Electrical Machines (SME), Andrychów, Poland, 10–13 June 2018.
17. Hoffelder, T. Equivalence analyses of dissolution profiles with the Mahalanobis distance. *Biom. J.* **2019**, *61*, 1120–1137. [CrossRef] [PubMed]
18. Xu, K. Fault Diagnosis Method of Power System Based on Neural Network. In Proceedings of the 2018 International Conference on Virtual Reality and Intelligent Systems (ICVRIS), Hunan, China, 10–11 August 2018.
19. Zhang, Y.; Shi, J.; Wang, S.; Zhan, Y. A Multi-source Information Fusion Fault Diagnosis Method for Vectoring Nozzle Control System Based on Bayesian Network. In Proceedings of the 2020 Asia-Pacific International Symposium on Advanced Reliability and Maintenance Modeling (APARM), Vancouver, BC, Canada, 20–23 August 2020.
20. Rao, T.S.; Ram, S.T.; Subrahmanyam, J. Neural network with adaptive evolutionary learning and cascaded support vector machine for fault localization and diagnosis in power distribution system. *Evol. Intell.* **2022**, *15*, 1171–1182.
21. Cai, B.; Lei, H.; Lin, J.; Xie, M. Bayesian Networks in Fault Diagnosis: Some research issues and challenges. In Proceedings of the 6th International Conference on Maintenance Performance Measurement and Management, Luleå, Sweden, 28 November 2016.
22. Gan, L.; Wu, H.; Fang, W. Bayesian network approach based on fault isolation for power system fault diagnosis. In Proceedings of the International Conference on Power System Technology, Chengdu, China, 20–22 October 2014.
23. Xu, L.; Zhou, Y. Fault diagnosis for BLDCM system used FFT algorithm and support vector machines. In Proceedings of the IEEE International Conference on Aircraft Utility Systems, Beijing, China, 10–12 October 2016.
24. Odavic, M.; Sumner, M.; Wheeler, P.; Jing, L. Real-time fault diagnostics for a permanent magnet synchronous motor drive for aerospace applications. In Proceedings of the Energy Conversion Congress & Exposition, Atlanta, GA, USA, 12–16 September 2010.
25. Chen, Q.; Li, W. Research on Fault Diagnosis Method of Aircraft Secondary Distribution System Based on Multi-valued Logic. In Proceedings of the International Conference on Sensing, San Diego, CA, USA, 12–14 June 2017.
26. Li, W.; Li, H.; Gu, S.; Chen, T. Process fault diagnosis with model- and knowledge-based approaches: Advances and opportunities. *Control Eng. Pract.* **2020**, *105*, 104637. [CrossRef]
27. Wang, C.; Li, J.; Zhu, X.; Xu, C.; Cheng, X. Adaptive Neural Fuzzy Petri Net Algorithm for Motor Fault Diagnosis. *IOP Conf. Ser. Earth Environ. Sci.* **2020**, *446*, 042063. [CrossRef]
28. Jiang, L.; Hua, Y.; Li, Q.; Zhang, R. Fault diagnosability qualitative analysis of spacecraft based on temporal fault signature matrix. In Proceedings of the Guidance, Navigation & Control Conference, Nanjing, China, 12–14 August 2016.
29. Liu, C.; Wu, G.; Yang, C.; Li, Y.; Wu, Q. A Fault Diagnosis Method Based on Signed Directed Graph and Correlation Analysis for Nuclear Power Plants. In Proceedings of the 2020 International Conference on Nuclear Engineering Collocated with the ASME 2020 Power Conference, Virtual, 4–5 August 2020.
30. Yu, J.; Wang, K.; Ye, L.; Song, Z. Accelerated Kernel Canonical Correlation Analysis with Fault Relevance for Nonlinear Process Fault Isolation. *Ind. Eng. Chem. Res.* **2019**, *58*, 18280–18291. [CrossRef]
31. Ye, Z.; Yan, H.; Zhao, Z.; Chen, Y.; Yang, Z. Research on Comprehensive Cascade Fault Diagnosis Technology for Vehicle Management System Actuator Control Subsystem Based on Associated Fault Mode Library. In Proceedings of the 2020 Prognostics and Health Management Conference (PHM-Besançon), Besançon, France, 4–7 May 2020.
32. Chai, Z.; Liu, C.; Zhu, M.; Han, Y. Fault Detection in Power Plant Equipment Based on Multi-sensor Data Correlation Analysis. *Comput. Digit. Eng.* **2019**, *47*, 682–688. [CrossRef]

33. Jun-Jie, X.U.; Chen, R. Probabilistic Diagnosis Approach to Diagnosing Multiple-fault Programs with Fault Correlation. *Comput. Sci.* **2017**, *44*, 124–130. [CrossRef]
34. Qi, H.; Xie, Q.; Yang, W.; Kan, S. Failure Mode, Effect and Criticality Analysis of Controllable Pitch Propeller Based on Fault Correlation. *Mech. Sci. Technol. Aerosp. Eng.* **2014**, *33*, 399–403.
35. Liu, H.; Pi, D.; Qiu, S.; Wang, X.; Guo, C. Data-driven identification model for associated fault propagation path. *Measurement* **2022**, *188*, 110628. [CrossRef]
36. Aini, A.; Salehipour, A. Speeding up the Floyd-Warshall algorithm for the cycled shortest path problem. *Appl. Math. Lett.* **2012**, *25*, 1–5. [CrossRef]
37. Kasa, Z. Warshall's algorithm-survey and applications. *Ann. Math. Et Inform.* **2021**, *54*, 17–31. [CrossRef]
38. Hadi, A.S.; Nyquist, H. Frechet distance as a tool for diagnosing multivariate data. *Linear Algebra Its Appl.* **1999**, *289*, 183–201. [CrossRef]
39. Gudmundsson, J.; Valladares, N. A GPU Approach to Subtrajectory Clustering Using the Fréchet Distance. *IEEE Trans. Parallel Distrib. Syst.* **2015**, *26*, 924–937. [CrossRef]
40. Tang, B.; Yiu, M.L.; Mouratidis, K.; Zhang, J.; Wang, K. On discovering motifs and frequent patterns in spatial trajectories with discrete Frechet distance. *Geoinformatica Int. J. Adv. Comput. Sci. Geogr.* **2022**, *26*, 29–66. [CrossRef]
41. Chua, L.O.; Roska, T. The CNN paradigm. *Circuits Syst. I Fundam. Theory Appl. IEEE Trans.* **1993**, *40*, 147–156. [CrossRef]
42. Lei, Y.; Yang, B.; Jiang, X.; Jia, F.; Li, N.; Nandi, A.K. Applications of machine learning to machine fault diagnosis: A review and roadmap. *Mech. Syst. Signal Process.* **2020**, *138*, 106587. [CrossRef]
43. Pan, L.; Ji, B.; Xi, P.; Wang, X.; Chongcheawchamnan, M.; Peng, S. FEDI: Few-shot learning based on Earth Mover's Distance algorithm combined with deep residual network to identify diabetic retinopathy. In Proceedings of the 2021 IEEE International Conference on Bioinformatics and Biomedicine (BIBM), Houston, TX, USA, 9–12 December 2021.
44. Yu, L.; Hao, C.; Duo, Q.; Qin, J.; Heng, P. Automated Melanoma Recognition in Dermoscopy Images via Very Deep Residual Networks. *IEEE Trans. Med. Imaging* **2016**, *36*, 994–1004. [CrossRef]
45. Shi, D.; Wu, Z.; Zhang, L.; Hu, B.; Meng, K. Multi-Scale Deep Residual Shrinkage Network for Atrial Fibrillation Recognition. *Int. J. Comput. Intell. Appl.* **2022**, *21*, 2250015. [CrossRef]
46. Pan, H.; You, X.; Liu, S.; Zhang, D. Pearson correlation coefficient-based pheromone refactoring mechanism for multi-colony ant colony optimization. *Appl. Intell.* **2021**, *51*, 752–774. [CrossRef]
47. Cui, F.; Tu, Y.; Gao, W. A Photovoltaic System Fault Identification Method Based on Improved Deep Residual Shrinkage Networks. *Energies* **2022**, *15*, 3961. [CrossRef]
48. Cw, A.; Jing, S.; Ld, A.; Yang, L.; Jia, C. Comprehensive benefit evaluation of solar PV projects based on multi-criteria decision grey relation projection method: Evidence from 5 counties in China. *Energy* **2021**, *238*, 121654.
49. Li, G.; Zhang, A.; Zhang, Q.; Wu, D.; Zhan, C. Pearson Correlation Coefficient-Based Performance Enhancement of Broad Learning System for Stock Price Prediction. *IEEE Trans. Circuits Syst. Ii-Express Briefs* **2022**, *69*, 2413–2417. [CrossRef]
50. Li, Z.; Zhao, H.; Zeng, R.; Xia, K.; Guo, Q.; Li, Y. Fault Identification Method of Diesel Engine in Light of Pearson Correlation Coefficient Diagram and Orthogonal Vibration Signals. *Math. Probl. Eng.* **2019**, *2019*, 2837580.
51. Liu, Y.; Mu, Y.; Chen, K.; Li, Y.; Guo, J. Daily Activity Feature Selection in Smart Homes Based on Pearson Correlation Coefficient. *Neural Process. Lett.* **2020**, *51*, 1771–1787. [CrossRef]
52. Garcez, T.V.; Cavalcanti, H.T.; Almeida, A. A hybrid decision support model using Grey Relational Analysis and the Additive-Veto Model for solving multicriteria decision-making problems: An approach to supplier selection. *Ann. Oper. Res.* **2021**, *304*, 199–231. [CrossRef]
53. Qu, W.; Chen, Z.; Wang, P.; Sun, J. A Grey Qualitative Based Approach for Environmental Information Analysis. *J. Grey Syst.* **2017**, *29*, 1–13.
54. Shi, C.-Z.; Zhao, Q.; Luo, L.-P. Application of Gray-scale Texture Feature In the Diagnosis of Pulmonary Nodules. In *SREE Workshop on Medical Materials and Engineering (WMME 2011)*; Trans Tech Publications Ltd.: Macau, China, 2012.
55. Xue, W.; Kuang, T. Image Edge Detection Based on Krisch Operator and Gray Correlation Analysis. In Proceedings of the 13th International Conference on Graphics and Image Processing (ICGIP), Kunming, China, 18–20 August 2021; Yunnan University: Kunming, China, 2022.
56. Cabana, E.; Lillo, R.E.; Laniado, H. Multivariate outlier detection based on a robust Mahalanobis distance with shrinkage estimators. *Stat. Pap.* **2021**, *62*, 1583–1609. [CrossRef]
57. Kwak, B.I.; Han, M.L.; Kim, H.K. Cosine similarity based anomaly detection methodology for the CAN bus. *Expert Syst. Appl.* **2021**, *166*, 114066. [CrossRef]
58. Deepa, N.; Khan, M.Z.; Prabadevi, B.; Vincent, D.R.P.M.; Maddikunta, P.K.R.; Gadekallu, T.R. Multiclass Model for Agriculture Development Using Multivariate Statistical Method. *IEEE Access* **2020**, *8*, 183749–183758. [CrossRef]
59. El Bendadi, K.; Lakhdar, Y.; Sbai, E.H. An Improved Kernel Credal Classification Algorithm Based on Regularized Mahalanobis Distance: Application to Microarray Data Analysis. *Comput. Intell. Neurosci.* **2018**, *2018*, 7525786. [CrossRef]
60. Omara, I.; Hagag, A.; Ma, G.; Abd El-Samie, F.E.; Song, E. A novel approach for ear recognition: Learning Mahalanobis distance features from deep CNNs. *Mach. Vis. Appl.* **2021**, *32*, 38. [CrossRef]
61. Keogh, E. Exact Indexing of Dynamic Time Warping—Science Direct. VLDB'02. In Proceedings of the 28th International Conference on Very Large Databases, Hong Kong, China, 20–23 August 2002; pp. 406–417.

62. Abdulhussain, M.I.; Gan, J.Q. An Experimental Investigation on PCA Based on Cosine Similarity and Correlation for Text Feature Dimensionality Reduction. In Proceedings of the 7th Computer Science and Electronic Engineering Conference (CEEC), England, UK, 24–25 September 2015.
63. Buciu, I.; Kotropoulos, C.; Pitas, I. Comparison of ICA approaches for facial expression recognition. *Signal Image Video Process.* **2009**, *3*, 345–361. [CrossRef]
64. Li, G.; Shen, J.; Dai, C.; Wu, H.; Becker, S.I. ShVEEGc: EEG Clustering With Improved Cosine Similarity-Transformed Shapley Value. *IEEE Trans. Emerg. Top. Comput. Intell.* **2022**, 1–15. [CrossRef]
65. Zhao, M.; Zhong, S.; Fu, X.; Tang, B.; Pecht, M. Deep Residual Shrinkage Networks for Fault Diagnosis. *IEEE Trans. Ind. Inform.* **2020**, *16*, 4681–4690. [CrossRef]
66. Adachi, Y.; Kawamoto, S.; Morishima, S.; Nakamura, S. Acoustic features for estimation of perceptional similarity. In Proceedings of the 8th Pacific Rim Conference on Multimedia, Hong Kong, China, 11–14 December 2007; City University of Hong Kong: Hong Kong, China.
67. Kim, S.-H.; Yang, H.-J.; Ng, K.S. Temporal Sign Language Analysis Based on DTW and Incremental Model. In Proceedings of the 9th IEEE Malaysia International Conference on Communications, Kuala Lumpur, Malaysia, 15–17 December 2009.
68. Wu, H.; Peng, Q.; Huang, Y. Features Extraction and Correlation Analysis of Stock Index. In Proceedings of the 8th World Congress on Intelligent Control and Automation (WCICA), Jinan, China, 6–9 July 2010.
69. Liu, Y.; She, G.-R.; Chen, S.-X. Magnetic resonance image diagnosis of femoral head necrosis based on ResNet18 network. *Comput. Methods Programs Biomed.* **2021**, *208*, 106254. [CrossRef] [PubMed]
70. Petrov, D.; Marshall, N.; Vancoillie, L.; Cockmartin, L.; Bosmans, H. Anthropomorphic ResNet18 for multi-vendor DBT image quality evaluation. In Proceedings of the Conference on Medical Imaging—Image Perception, Observer Performance, and Technology Assessment, Medical Imaging, Houston, TX, USA, 19–20 February 2020.
71. Zhou, Z.; Ma, Z.; Wang, Y.; Zhu, Z. Fabric wrinkle rating model based on ResNet18 and optimized random vector functional-link network. *Text. Res. J.* **2022**. [CrossRef]
72. Du, T.; Zhang, H.; Wang, L. Analogue circuit fault diagnosis based on convolution neural network. *Electron. Lett.* **2019**, *55*, 1277–1278. [CrossRef]
73. Senanayaka, J.S.L.; Van Khang, H.; Robbersmvr, K.G. CNN based Gearbox Fault Diagnosis and Interpretation of Learning Features. In Proceedings of the 30th IEEE International Symposium on Industrial Electronics (ISIE), Kyoto, Japan, 20–23 June 2021.